Online Supporting Information for

Substitution of a Hydroxamic Acid Anchor into the MK-2 Dye for Enhanced Photovoltaic Performance and Water Stability in a DSSC

Christopher Koenigsmann,[1] Bradley J. Brennan,[1] Christian F.A. Negre,[1] Matthieu Koepf,[1] Alec C. Durrell,[1] Rebecca L. Milot,[1] V. S. Batista,[1] G. W. Brudvig,[1] R. H. Crabtree,[1] and C. A. Schmuttenmaer[1]

[1]Yale Energy Sciences Institute and Department of Chemistry,
Yale University, New Haven, CT 06520-8107, United States

Teresa S. Ripolles,[2] Jose A. Torre,[2] Juan Bisquert[2,3]

[2]Photovoltaic and Optoelectronic Devices Group, Departament de Física,
Universitat Jaume I, 12071 Castelló, Spain

[3]Department of Chemistry, Faculty of Science, King Abdulaziz University, Jeddah, Saudia Arabia

Contents:

1. Synthesis & Characterization of the MK-2THP, MK-2HA and MK-2E dyes

Materials: MK-2 dye (2-Cyano-3-[5‴-(9-ethyl-9*H*-carbazol-3-yl)-3′,3″,3‴,4-tetra-*n*-hexyl-[2,2′,5′,2″,5″,2‴]-quater thiophen-5-yl] acrylic acid, 95%) was obtained from Sigma Aldrich. O-(Tetrahydro-2H-pyran-2-yl)hydroxylamine (THP) was synthesized according to the procedure previously described by Patel and co-workers.[1] *N,N,N′,N′*-Tetramethyl-*O*-(1*H*-benzotriazol-1-yl) uronium hexafluorophosphate (HBTU) was purchase from Alfa Aesar (99%). N,N-diisopropylethylamine (DIEPA) was distilled over KOH prior to use. Tetra-*n*-butylammonium hexafluorophosphate ($TBAPF_6$) was obtained from Alfa Aesar and purified by recrystallization from boiling ethanol. Other chemicals and reagents were obtained from commercial sources. Silica gel chromatography was performed using SiliaFlash F60 (40-63 μm, 60Å) obtained from Silicycle.

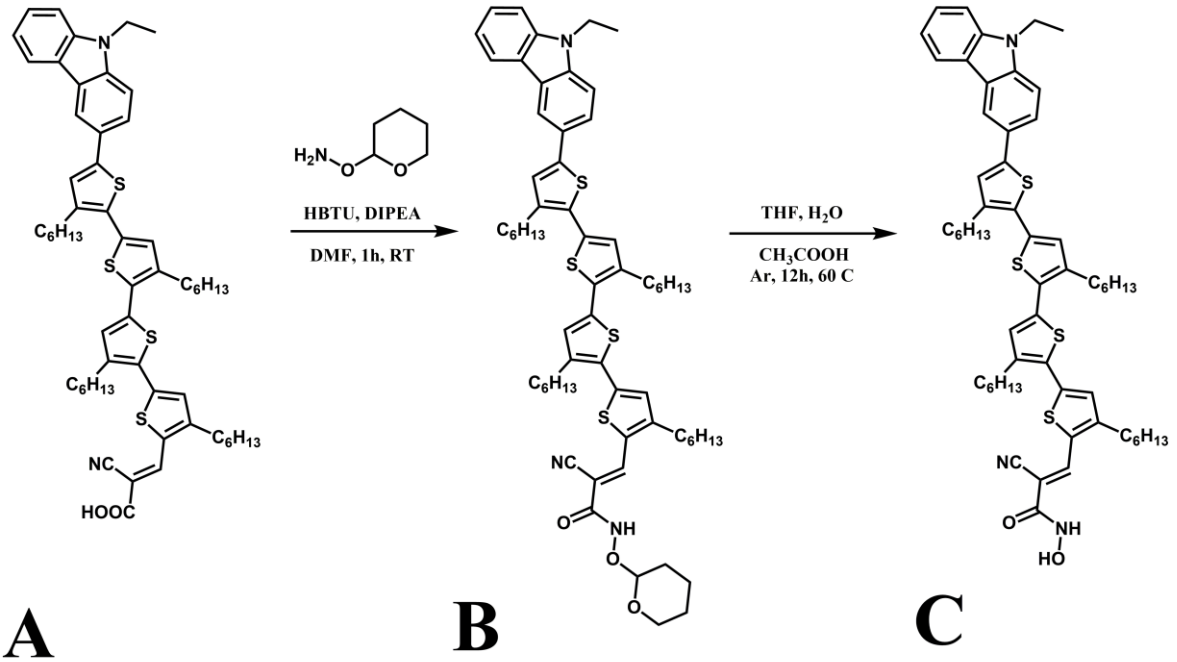

Scheme S1. Synthetic steps for the production of MK-2THP (B) and MK-2HA (C) from the commercial MK-2 dye (A).

Synthesis & Characterization of MK-2THP: The synthesis of the protected hydroxylamine derivatized MK-2 (MK-2THP) dye from commercial MK-2 dye is summarized in Scheme S1. Initially, the MK-2 dye (30 mg, 0.032 mmol) was dissolved in N,N dimethylformamide (2 mL) in presence of DIEPA (10.2 μL, 7.6 mg, 0.059 mmol). HBTU (15 mg, 0.040 mmol) was added to the solution and the mixture was stirred at room temperature, for 5 minutes before adding NH_2-OTHP (18 mg, 0.154 mmol). The reaction mixture was then stirred at room temperature in the dark. After 1 h, the mixture was poured into water (50 mL). Brine was added (15 mL) and the aqueous phase was extracted with diethyl ether (3 x 50 mL). The organic layers were combined, washed with water (3 x 50 ml), dried over anhydrous Na_2SO_4, filtered and the solvent was evaporated under reduced pressure. The crude residue was purified by column chromatography using dichloromethane eluent. The desired product MK-2THP (28 mg, 77%) was obtained as the fourth eluted band.

^{1}H NMR (400 MHz, $CDCl_3$, δ) 8.89 (1H, br s), 8.50 (1H, s), 8.31 (1H, d, *J* = 1.8 Hz), 8.14 (1H, d, *J* = 7.6 Hz), 7.72 (1H, dd, *J* = 8.5, 1.8 Hz), 7.51 – 7.47 (1H, m), 7.42 (1H, d, *J* = 5.7 Hz), 7.39 (1H, d, *J* =

5.6 Hz), 7.28 –7.24 (1H, m), 7.20 (1H, s), 7.08 (1H, s), 7.02 (2H, s), 5.09 – 5.07 (1H, m), 4.39 (2H, q, *J* = 7.3 Hz), 4.05 – 4.00 (1H, m), 3.71 – 3.67 (1H, m), 2.88 – 2.80 (8H, m), 1.98 – 1.80 (2H, m), 1.76 – 1.61 (12H, m), 1.48 –1.44 (9H, m), 1.39 – 1.31 (18H, m), 0.92 – 0.88 (12H, m). $\lambda_{max}(CH_2Cl_2)$/nm 307, 384, 489. HRMS–MALDI-TOF (*m/z*): M^+ calcd for $C_{63}H_{79}N_3O_3S_4$, 1053.5004; found, 1053.4979.

Synthesis & Characterization of MK-2HA: The preparation of MK-2HA from the MK-2THP precursor is summarized in Scheme S1. MK-2THP dye (26 mg, 0.025 mmol) was dissolved in a mixture of tetrahydrofuran (THF) / water / acetic acid (7:2:1, 15 mL) and the solution was purged with argon (3 vacuum/argon cycles). The solution was stirred under argon in the dark at 60 ºC. The reaction progress was followed by TLC (SiO_2, CH_2Cl_2). When no starting material remained (ca. 12 h) the tetrahydrofuran was evaporated and the residual aqueous phase diluted with 20 mL of a 5% $NaHCO_3$ aqueous solution. The aqueous layer was extracted with diethyl ether (3 x 25 mL). The organic layers were combined, dried with Na_2SO_4, filtered, and the solvent was evaporated under reduced pressure to yield the desired product MK-2HA (22 mg, 92%).
^{1}H NMR (400 MHz, $CDCl_3$, δ) 8.88 (1H,br s), 8.45 (1H, s), 8.31 (1H, d, *J* = 1.8 Hz), 8.14 (1H, d, *J* = 7.6 Hz), 7.72 (1H, d, *J* = 8.4), 7.52 – 7.47 (1H, m), 7.43 – 7.40 (2H, m), 7.28 –7.24 (1H, m), 7.20 (1H, s), 7.09 (1H, s), 7.02 (2H, s), 4.39 (2H, q, *J* = 7.2 Hz), 2.89 – 2.80 (8H, m), 1.76 – 1.63 (8H, m), 1.48 –1.43 (9H, m), 1.37 – 1.33 (18H, m), 0.93 – 0.91 (12H, m). λ_{max}(toluene)/nm 310 (ε/dm^3 mol^{-1} cm^{-1} 18 800), 385 (19 500), 490 (29 400). HRMS–MALDI-TOF (*m/z*): M^+ calcd for $C_{58}H_{71}N_3O_2S_4$, 969.4429; found, 969.4275.

Synthesis & Characterization of MK-2E: The synthesis of the MK-2E is summarized in Scheme S2. Potassium carbonate (0.072 mmol) and 20 µL (0.015 mmol) of a 5 vol% iodomethane solution prepared in DMF was added to a solution consisting of 14 mg (0.015 mmol) MK-2 dissolved in 4 mL of DMF. The mixture was stirred at room temperature for 3 h and subsequently transferred to a separatory funnel with 20 mL of chloroform. The organic layer was washed with 20 mL of aqueous citric acid, twice with 20 mL H_2O, and dried under reduced pressure. The crude mixture was purified by silica gel chromatography using dichloromethane eluent, and the first eluted band was dried under reduced pressure to obtain MK-2E (9 mg, 63%) as a red solid.
^{1}H NMR (400 MHz, $CDCl_3$, δ) 8.40 (1H, s), 8.31 (1H, d, *J* = 1.6 Hz), 8.13 (1H, d, *J* = 7.7 Hz), 7.72 (1H, dd, *J* = 8.5 Hz, 1.8 Hz), 7.49 (1H, m), 7.41 (2H, m), 7.26 (1H, m), 7.20 (1H, s), 7.09 (1H, s), 7.02 (2H, s), 4.38 (2H, q, *J* = 7.3 Hz), 3.91 (3H, s), 2.89 - 2.79 (8H, m), 1.79 - 1.62 (8H, m), 1.51 - 1.36 (8H, br m), 1.46 (3H, t, *J* = 7.2 Hz), 1.42 - 1.29 (16H, m), 0.94 - 0.89 (12H, m). $\lambda_{max}(CH_2Cl_2)$/nm 309, 384, 493. HRMS–MALDI-TOF (*m/z*): M^+ calcd for $C_{59}H_{72}N_2O_2S_4$, 968.4477; found, 968.4476.

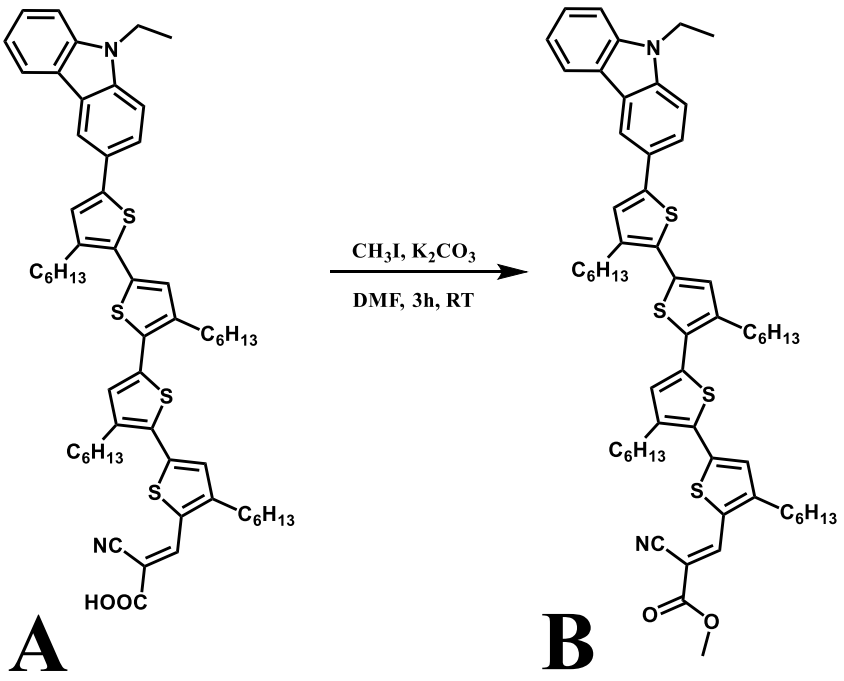

Scheme S2. Synthetic steps for the production of MK-2E (B) from commercial MK-2 dye (A).

Characterization Methods: UV-Visible spectroscopy was performed using a Shimadzu UV-2600 or Cary 50 spectrometer. Extinction coefficients of MK-2, MK-2HA, and N719 were obtained in toluene, DMF, DMF/water and THF for the protonated acids. Spectra of deprotonated dyes were obtained by adding 10 µL of 1 M tetra-*n*-butylammonium hydroxide (TBAH) in methanol to the protonated dye solution in 4 mL of solvent. Extinction coefficients are reported with a precision of ± 10% of the measured value. Proton NMR spectra were collected on a 400 MHz instrument in $CDCl_3$ with internal TMS standard. Coupling values (*J*) are reported in Hz and chemical shifts are reported as δ ppm from TMS. Mass spectrometry was performed with an Agilent Voyager DE Pro MALDI-TOF mass spectrometer.

Steady-state and Time-Correlated Single Photon Counting (TCSPC) spectrofluorimetry was performed in dichloromethane solvent using a Horiba FluoroLog (FL3-21) instrument with Fluorohub TCSPC accessory and TBX-04 detector. Uncorrected steady-state spectra were obtained by illuminating at 459 nm with sample absorption below 0.08 absorbance units. TCSPC was performed using a 459 nm nanoLED pulsed excitation with 1.2 ns instrument response time. Fitting of the data was performed with the DAS6 software provided by Horiba.

Electrochemistry was performed with either a Pine WaveNow-XV or Gamry Reference 600 potentiostat. Working and counter electrodes were platinum, with a pseudo Ag/AgCl reference. Electrolyte consisted of 100 mM tetra-*n*-butylammonium hexafluorophosphate in dichloromethane. All data are referenced to the normal hydrogen electrode (NHE) using the ferrocene redox couple (0.72 V vs. NHE) as an internal reference. Electrochemical characterization was performed on the protected MK-2THP and MK-2E analogs to avoid deleterious interactions of the carboxylate groups in MK-2 and MK-2HA molecules with the platinum electrode.

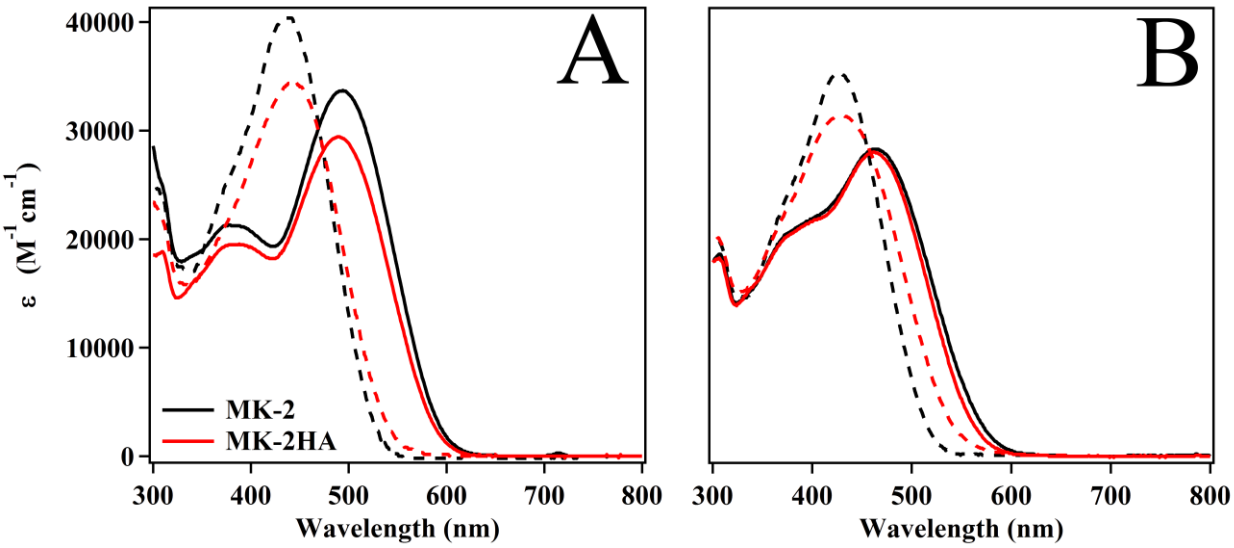

Figure S1. UV-visible spectra of the MK-2 (black trace) and MK-2HA (red trace) obtained in toluene (A) and THF (B). Spectra were obtained in pure solvent (solid traces) and in solutions of tetrabutylammonium hydroxide (dashed traces).

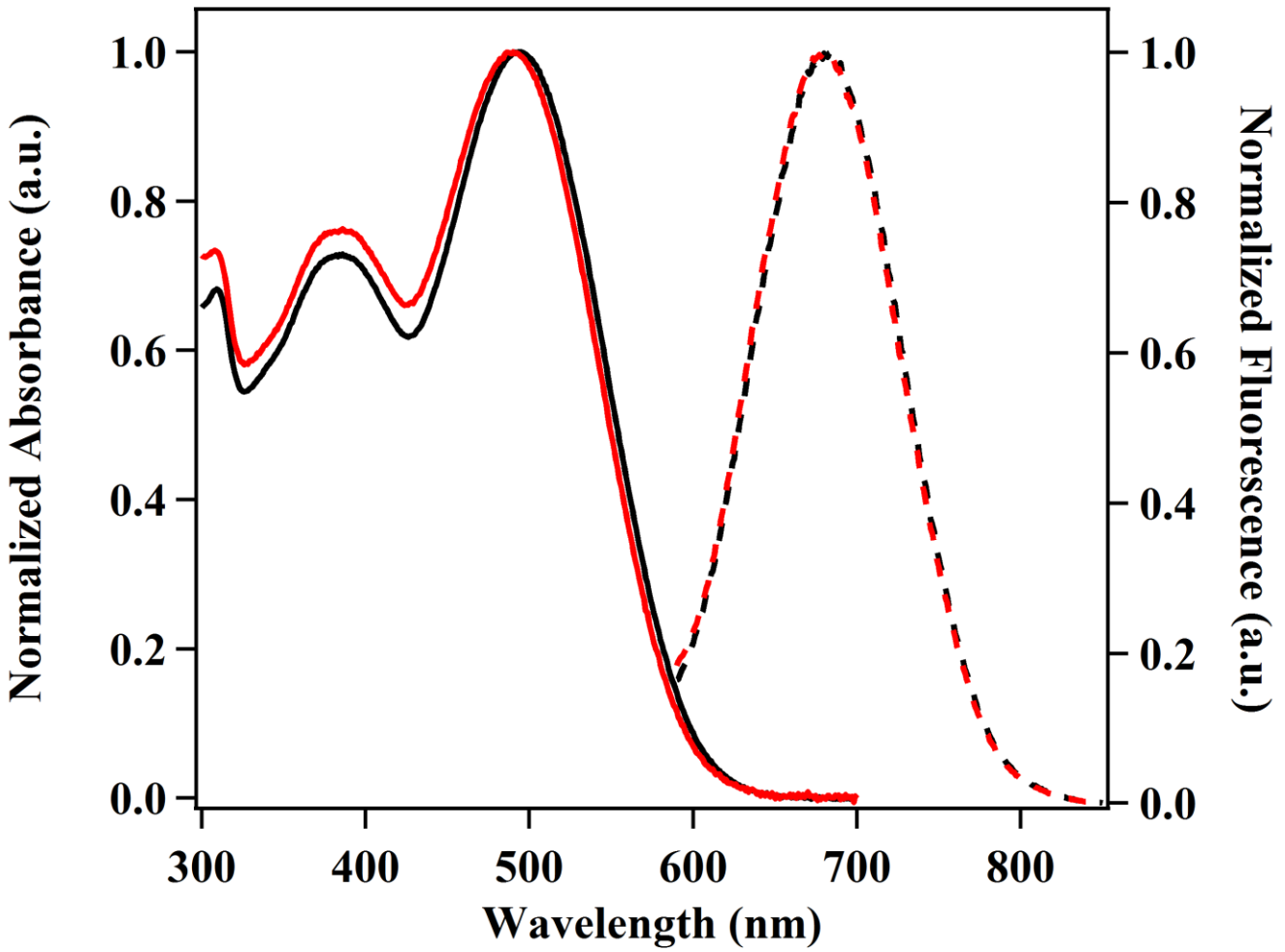

Figure S2. UV-visible (solid traces) and fluorescence (dashed traces) spectra for the MK-2E (black traces) and MK-2THP (red traces) obtained from solutions of the dyes prepared in dichloromethane. Spectra were normalized to the maximum measured absorbance and emission values for ease of comparison.

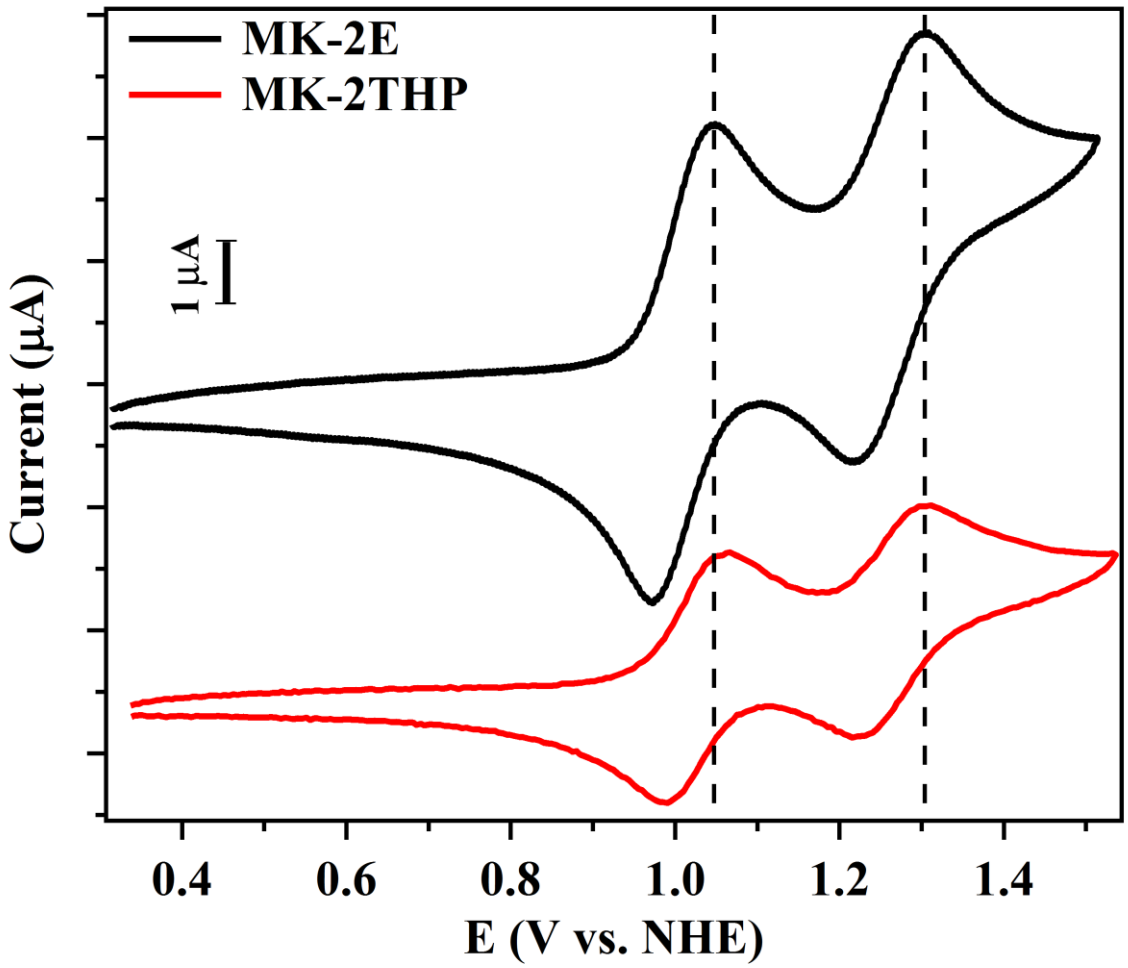

Figure S3. Cyclic voltammograms obtained from solutions of MK-2E and MK-2THP at a scan rate of 50 mV/s. The vertical lines denote the oxidation peak potentials of the MK-2E dye for the purpose of comparison.

2. Characterization of Photoelectrochemical Properties in Dye Sensitized Solar Cells

The assembly of the functional dye sensitized solar cell devices was based on previously reported methods.[2] Transparent conductive fluorine:SnO_2 glass (FTO, 7 Ω/square, Hartford Glass) was used as electrodes for the TiO_2 thin film working electrode and the counter electrode. Prior to deposition of the TiO_2 films, the FTO was pre-treated by immersing in a solution of 40 mM titanium (IV) chloride − THF complex (Acros Organics, 99.9%) at 75 °C for a period of 30 min. The treated films were calcined at 370 °C and 570 °C for periods of 5 min and 30 min, respectively. The TiO_2 films were prepared with two different TiO_2 nanoparticle pastes with sizes of 15 − 20 nm (transparent TiO_2 layer) and up to 450 nm (scattering TiO_2 layer) obtained from Solaronix (14411, T-SP) and Dyesol (18NR-AO), respectively. The deposition of the films was accomplished by doctor-blading yielding reproducible thickness of 15 µm for the transparent TiO_2 layer and 10 µm for the scattering TiO_2 layer after annealing at 370 °C for a period of 10 min and 470 °C for a period of 30 min. The as-prepared films were subsequently treated with $TiCl_4$ in an analogous fashion to the pre-treatment of the FTO glass. As-prepared films were sensitized in solutions consisting of 0.3 mM of the appropriate organic dye dissolved in anhydrous toluene for a period of either 16 or 24 hrs forming the final working electrodes. The N719 films were prepared by immersion into a solution of 0.7 mM N719 dye and 0.7 mM chenodeoxycholic acid prepared in anhydrous ethanol. Counter electrodes were prepared on FTO glass by depositing a solution of chloroplatinic acid (H_2PtCl_6) prepared in ethanol onto the surface followed by a heat treatment to crystallize the platinum at 450 °C for a period of 30 min.

Functional devices were prepared by sealing the working and counter electrodes together utilizing a 60 µm thick hot-melt film spacer (Surlyn) serving as both a sealant and spacer. In Section 3.2, Electrolyte A was prepared from a combination of 1,2-dimethyl-3-propylimidazolium iodide (DMPII, TCI, 0.6 M), lithium iodide (anhydrous, 99.95%, Alfa Aesar, 0.1 M), iodine (pure, Acros Organics, 0.2 M), 4-*tert*-butylpyridine (TBP, Sigma-Aldrich, 0.5 M) and anhydrous acetonitrile as the solvent (Omni Solv, EMD Millipore). This electrolyte formulation is based on previously reported results with the MK-2 dye and is optimized to give the best cell performance for the MK-2 dye. For the sake of consistency, we employ this same electrolyte formulation for the control cells based on the N719 dye. However, it should be noted that the high I_2 concentration of 0.2 M in electrolyte A is higher than the concentration typically utilized for N719 (0.03 – 0.05 M) and is known to cause a limitation of electron transport by the I_3^- species, which contributes to lower than expected fill-factor (*FF*) for this dye. The electrolyte solution was introduced into the cell by means of vacuum back-filling through a hole pre-drilled into the counter electrode. Prior to use the hole in the counter electrode was sealed with a glass cover slip and hot-melt film. The active area of each cell was 0.25 cm^2 (*i.e.* 0.5 x 0.5 cm^2). In this report, the j-V curves were performed without a mask and therefore, the measured J_{sc} values in this report will be 10 – 15% higher than those typically obtained if a mask were to be employed.

In the case of the water durability studies presented in Section 3.6, the electrolyte formulation B contained 2 M methyl-3-propylimidazolium iodide (MPII), 0.1 M LiI, 0.2 M I_2, 0.5 M TBP in acetonitrile. The concentration of the methyl-3-propylimidaolium iodide (MPII) was increased from 0.6 M in the standard formulation to 2 M in the water stability studies because of its ability to act as a surfactant and suitably co-solubilize the 4-*tert*-butylpyridine (TBP), iodine and water. Although useful for studying water content, the electrolyte employed in the water studies is significantly different from the optimized electrolyte for MK-2 dyes[3] employed in Section 3.2 and, thus, the measured efficiencies are considerably decreased. However, the overall trends in the device parameters are useful for evaluating the performance of functioning devices with up to 20% water purposefully added to the electrolyte.

3. Photoelectrochemical Performance & Impedance Spectroscopy of MK-2 Dye as a Function of Surface Linker

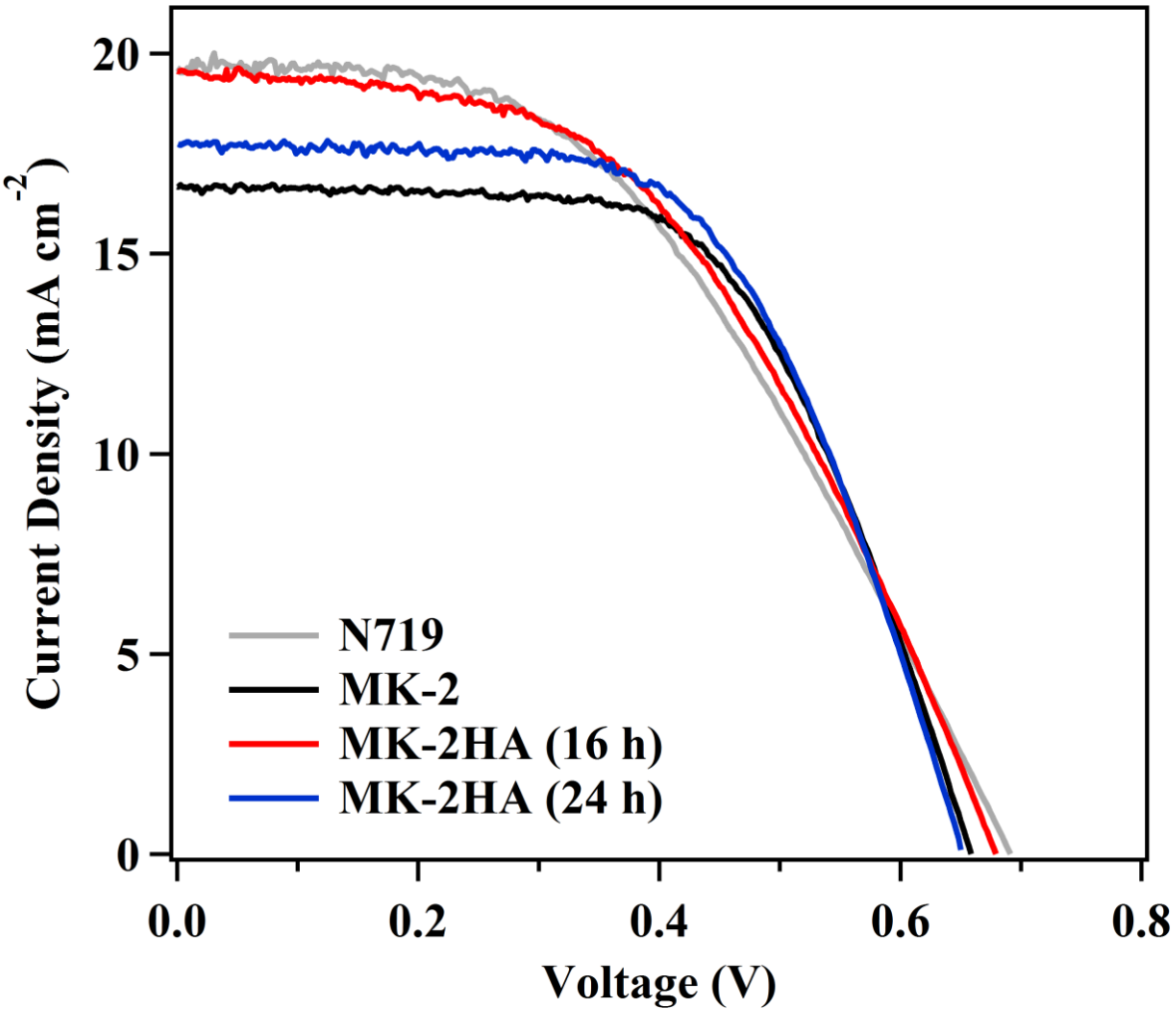

Figure S4. Current density vs. voltage curves (*j*-*V*) for DSSC devices prepared with electrolyte A and sensitized with N719 (gray), MK-2 (black), MK-2HA after adsorption for 16 h (red) and MK-2HA after adsorption for 24 h (blue), with organic electrolyte, under simulated one-sun illumination (AM1.5G).

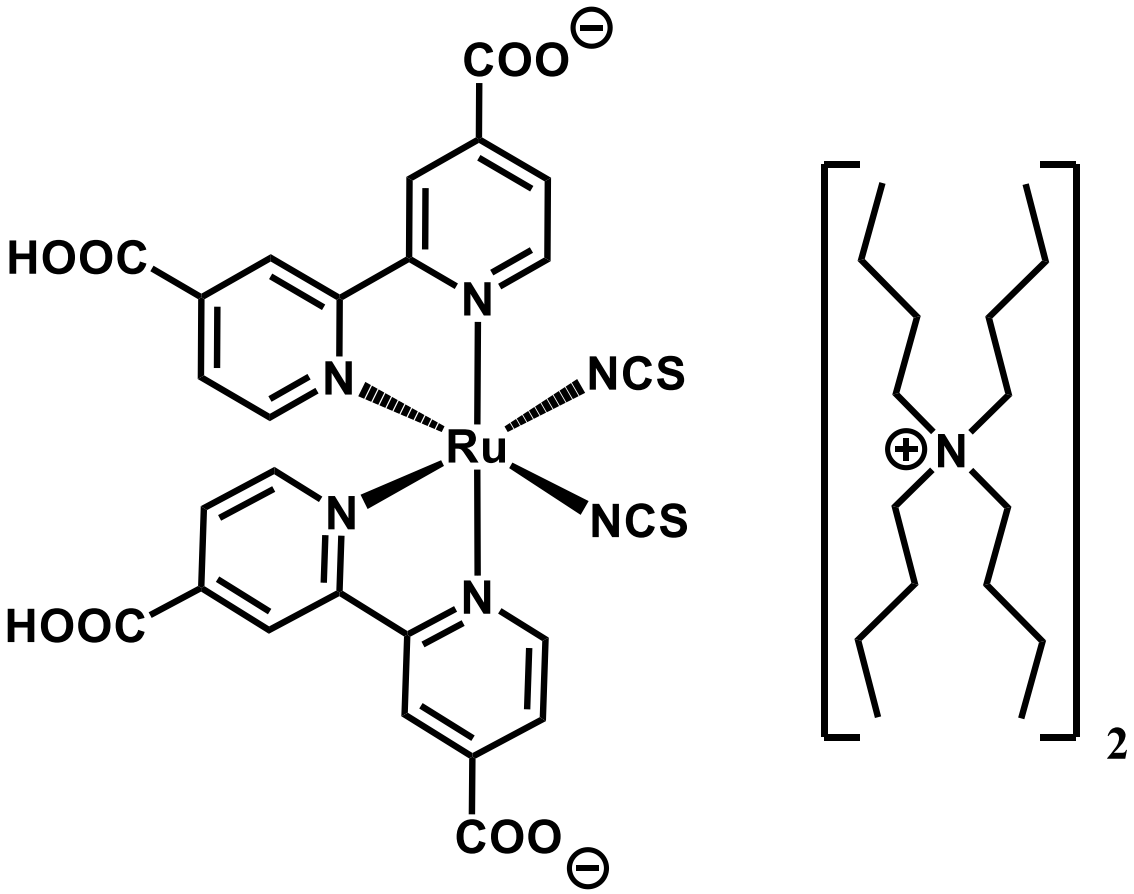

Figure S5. Structure of the N719 (di-tetrabutylammoniumcis-bis(isothiocyanato)bis(2,2'-bipyridyl-4,4'-dicarboxylato)ruthenium(II)) dye.

4. Injection and Recombination Dynamics of MK-2 and MK-2 Hydroxamate Sensitized Films

Analysis of Transient Absorption Spectroscopy Data: The lifetime of the charge-separated state was determined from the transient absorption (TA) data utilizing methods previously described in the literature.[4] The (TA) profiles were fit with a stretched exponential function shown in Equation 1 to determine the τ and β parameters. The refined parameters were then used to calculate the first moment of the Kohlrausch-William-Watts function $\langle \tau_{ww} \rangle$ using Equation 2, which provides a representative lifetime of the charge-separated state.

$$\Delta \mathrm{OD}_t = A \exp\left(\frac{t - t_0}{\tau} \right)^{\beta} \tag{1}$$

$$\langle \tau_{ww} \rangle = \left[\frac{\tau}{\beta} \Gamma\left(\frac{1}{\beta} \right) \right]^{-1} \tag{2}$$

Where Γ is the gamma function.

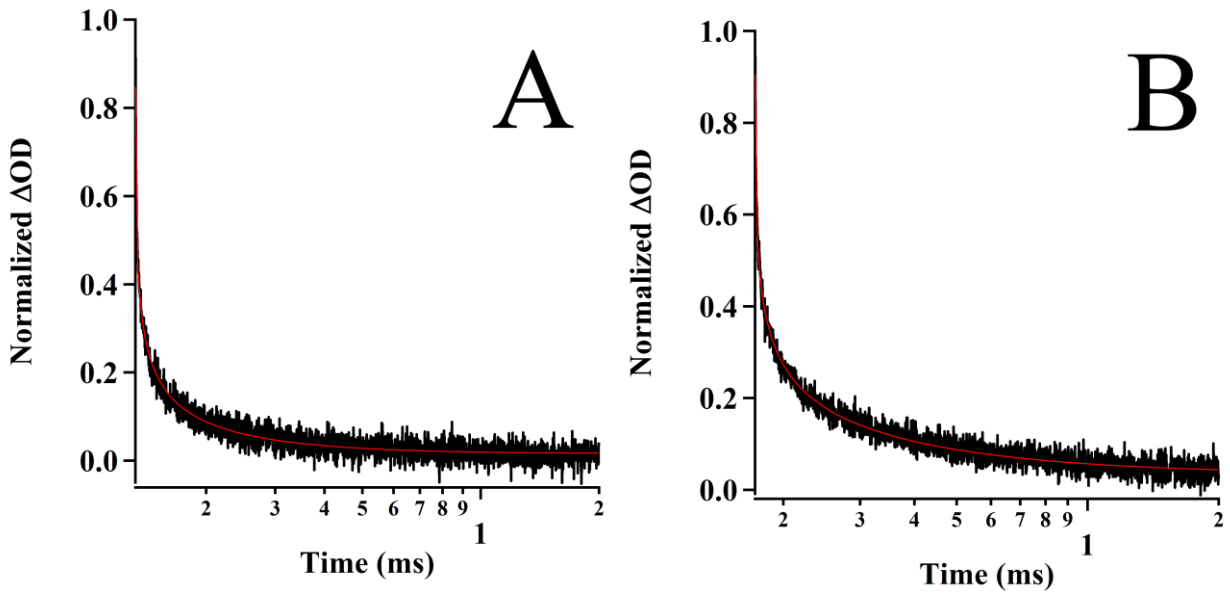

Sensitizer	τ	β	τ_{ww}
	μs		μs
MK-2	3.01 ± 0.06	0.311 ± 0.003	23.9
MK-2HA	7.9 ± 0.1	0.293 ± 0.002	81.9
N719	1.18 ± 0.02	0.212 ± 0.001	87.2

Figure S6. Fits of the MK-2 (A) and MK-2HA (B) transient absorption traces collected in acetonitrile utilizing a stretched exponential function. Immediately below is a table summarizing the lifetime (τ) and stretching (β) parameters determined from the fits. These values were utilized to calculate $\langle \tau_{ww} \rangle$ utilizing previously reported methods.[4]

5. Computational Procedures

Geometry Optimizations: In order to study the anchoring mode of MK-2 and MK-2HA onto TiO_2 nanoparticles, we employed Density Functional Theory (DFT) calculations of the Dye sensitized TiO_2 anatase (101) surface. Benzoic acid and phenyl-hydroxamic acid were employed in the case of the MK-2 and MK-2HA to model how these dyes anchor to the surface, while also minimizing the corresponding computational cost. The resulting anchoring configurations were then used as a template to attach MK2 and MK-2HA dyes, respectively. We base this approach on a similar previously used approach,[5] wherein a defect bidentate "O-vacancy" adsorption mode was employed for the attachment of both benzoic and phenyl-hydroxamic acid. Prior results demonstrate that this anchoring geometry minimizes the steric interactions between the adsorbate and the surface and is the most energetically favorable binding mode.[5] In the case of the carbonyl anchoring group, the Ti-OH bond that is formed is necessary in order to maintain a zero formal charge since an H atom is removed from the COOH anchoring group and O atom is removed from the Ti-O-Ti row. In the case of the hydroxamic acid anchoring group, we employ the "double deprotonated" anchoring mode (i.e. both OH and NH groups are deprotonated). A detailed computation analysis in a prior report[5, 6] has demonstrated this to be the most energetically favorable adsorption and in this case an H_2O molecule coordinates with a surface Ti atom.

The TiO_2 NP was modeled as an anatase (101) slab consisting of four layers of Ti^{4+} ions and eight layers of O^{2-} ions. An initial slab was constructed employing the crystallographic parameters (a = b = 3.7845 Å and c = 9.5143 Å) and crystal structure based on a previous report,[7] and was periodically replicated in two dimensions employing periodic boundary conditions. The super cell dimensions are 10.239 Å × 15.137 Å in the $[10\bar{1}]$ and [010] directions, respectively. A vacuum spacer of 10 Å was included to separate periodic slabs in the $[10\bar{1}]$ direction. The periodic DFT calculations were performed using the SIESTA computational package.[8] Electron exchange and correlation were described using the PBE implementation[9] of the generalized gradient approximation (GGA) functional, and a 200 eV mesh cutoff was employed. Only the Gamma point was used to integrate over the Brillouin zone. The geometry of the adsorbate and TiO_2 slab where relaxed to its minimum energy configuration (0.04 eV/Å cut off). The lower layer of Ti^{4+} plus the O^{2-} layers beneath them where fixed during all the optimization (Figure S7A).

MK-2 and MK-2HA where optimized separately using the DFT(B3LYP/631-G) level of theory as implemented in Gaussian09[10] and further attached following the patterns of the model anchoring groups. Frontier orbital analysis shows that both HOMO and LUMO symmetries as well as the E(LUMO)-E(HOMO) energy gap changes are minimal with the incorporation of hydroxamic anchor in MK-2 dye. These orbitals are shown in Figure S8.

IET simulations: A concise overview of the methodology employed to simulate the interfacial electron transfer (IET) is provided herein; however, a detailed discussion can be found in prior reports.[11] The electronic structure was represented *via* the Extended-Hückel (EH) Hamiltonian. The ground state electronic structure of the system is obtained after solving the time-independent Schrödinger equation in the Slater atomic orbital's basis set $\{|\chi_i\rangle\}$, where $\boldsymbol{H}$ is the EH Hamiltonian and $\boldsymbol{S}$ is the overlap matrix (Equation 3). $\boldsymbol{Q}$ and $\boldsymbol{E_q}$ represent the eigenvector and eigenvalues, respectively, of the q^{th} molecular orbital: $|\boldsymbol{q}\rangle = \sum_{\mathbf{i}} \mathbf{Q_i} |\boldsymbol{\chi_i}\rangle$.

$$\boldsymbol{HQ^q} = \boldsymbol{E_q SQ^q} \qquad (3)$$

The prepared initial state is expanded as a combination of molecular orbitals and can be further expanded with atomic orbitals (Equation 4). The propagation of the initial state was performed as shown in Equation 5, where Equation 6 is employed for B_i (t).

$$\left|\Psi_0\right\rangle = \sum_q C_q \left|q\right\rangle = \sum_{q,i} C_q Q_i^q \left|\chi_i\right\rangle \tag{4}$$

$$\left|\Psi(t)\right\rangle = e^{-\left(\frac{i}{\hbar}Ht\right)}\left|\Psi_0\right\rangle = \sum_i B_i(t)\left|\chi_i\right\rangle \tag{5}$$

$$B_i(t) = \sum_{i,q} C_q Q_i^q e^{-\frac{i}{\hbar}E_q t} \tag{6}$$

We have employed an integration time step of 1 fs for all the calculations in this work. In order to obtain the survival probability, the time dependent wave function was projected onto the atomic orbitals of the molecular adsorbate. In this case, the summation over '*i*' runs through the atomic orbitals of the adsorbate, and the simulation over '*j*' runs over the complete basis set. The function *P*(*t*) (Equation 7) is the probability that the photoelectron remains in the adsorbate molecule at time '*t*'.

$$P(t) = \sum_i^{adb}\sum_j^{all} B_i^* B_j(t) S_{ij} \tag{7}$$

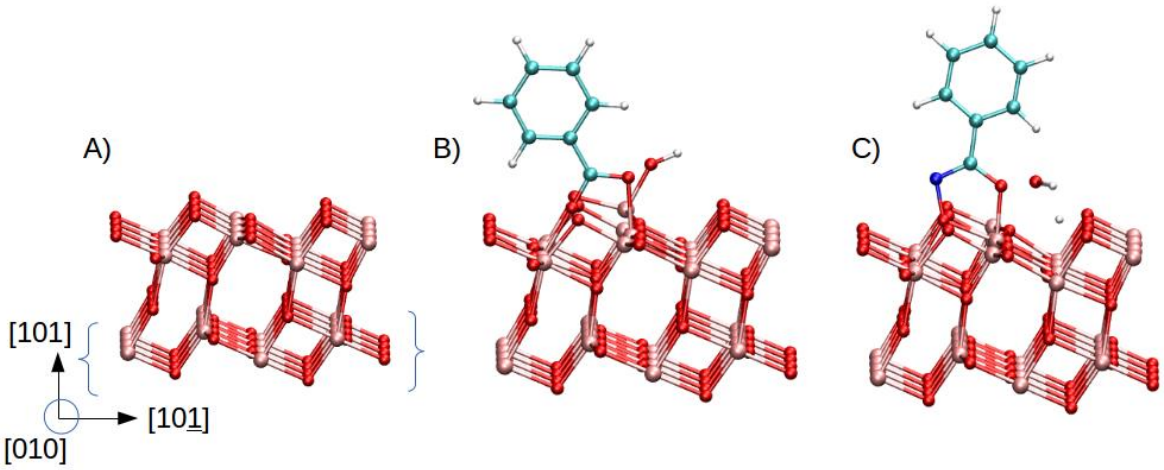

Figure S7. DFT optimized anatase TiO_2 (101) slab (A). Optimized structures for the anatase with benzoic acid (B) and phenyl-hydroxamic acid (C) are also depicted. The fixed layer of atoms is indicated by the curly brackets in A.

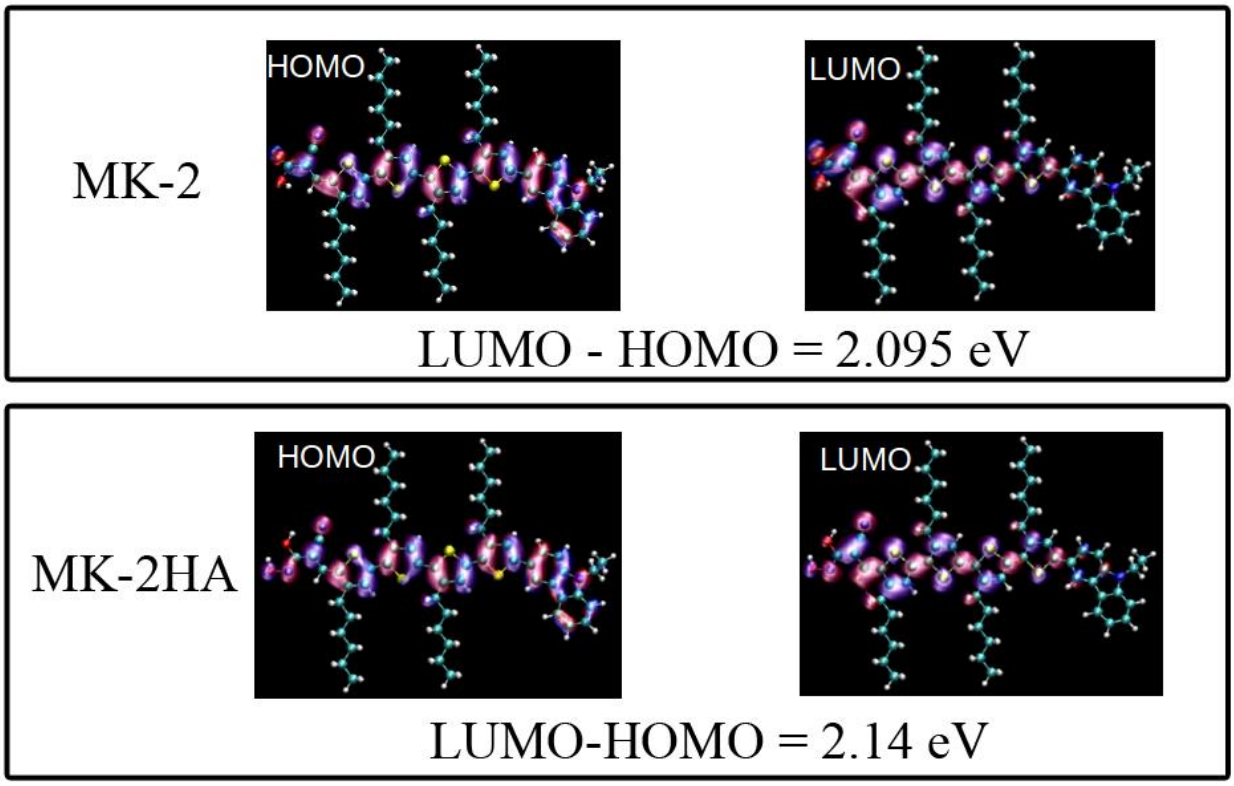

Figure S8. Frontier orbitals for MK-2 (top) and MK-2HA (bottom) are shown with the corresponding, calculated HOMO-LUMO energy gap values. The C, N, O, S, and H atoms are represented by light blue, blue, red, yellow and white spheres, respectively.

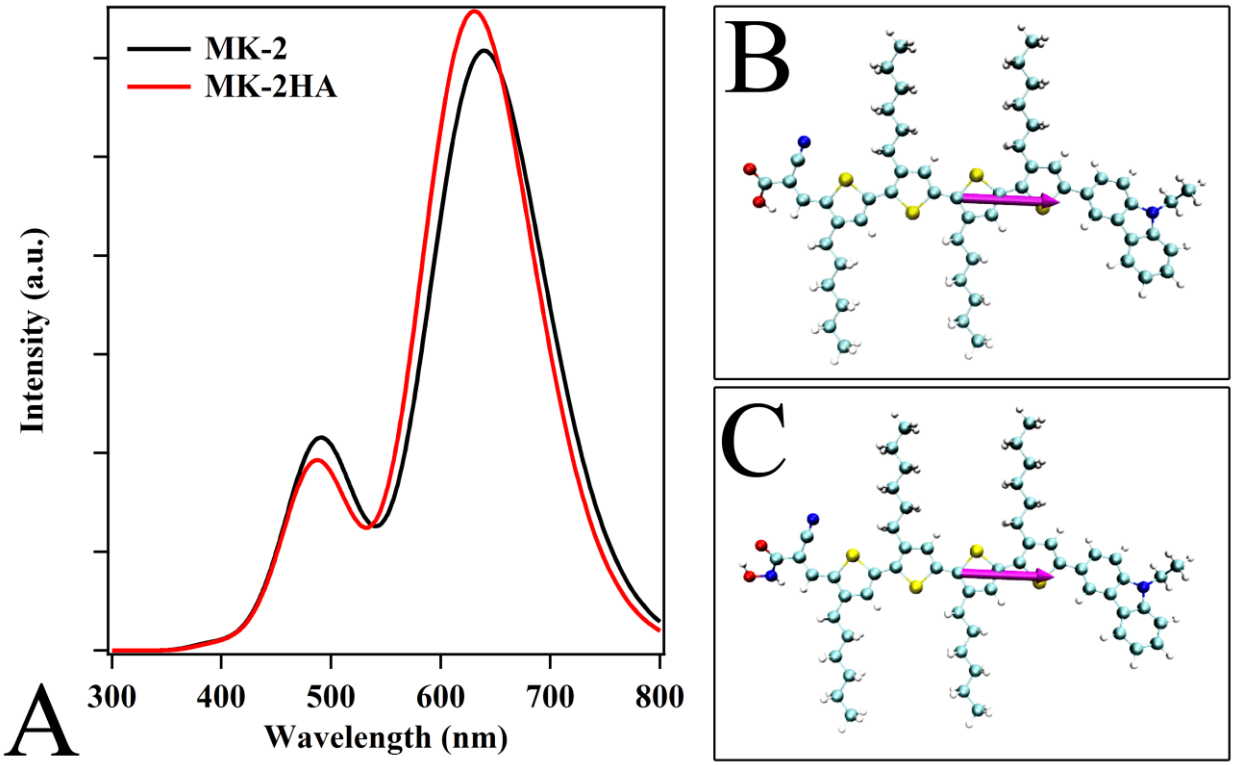

Figure S9. TDDFT calculated UV-visible absorption spectra for the MK-2 (black trace) and MK-2HA (red trace). The calculated transition dipole moment for the lowest energy band is shown in magenta overlaying the structure of the MK-2 (B) and MK-2HA (C).

6. Water Stability & Durability of Sensitized Films as a Function of Anchoring Group

Additional Details on Desorption Method: Examining the water stability of organic dyes can be challenging since the solubility of the MK-2 dye is minimal in acetonitrile and valeronitrile, which represent the principle components of the electrolyte in DSSCs. Thus, the hydrolysis of the surface anchoring groups in acetonitrile results in aggregation of the desorbed dye on the surface of the semiconductor and renders accurate measurements of the desorption rate difficult.[12] We overcome this issue by rationally employing DMF as the desorption solvent owing to its unique ability to co-solubilize the MK-2 dyes and water. In fact, spectroscopic analysis of mixtures of MK-2 dye and water confirm that the dye can remain soluble without measureable aggregation at concentrations of up to 35% water. In essence, the DMF/H_2O solvent system represents a "worst-case-scenario" since the hydrolysis of the surface anchoring group results in rapid desorption and solubilization of the dye into the solution.

Analysis of Desorption Data: The desorption data plotted as the concentration of dye desorbed with respect to desorption time (Figure S10) were fit assuming a first-order desorption process described by Equation 8. Specifically, the desorption is modeled by the ideal first-order desorption equation, *i.e.* $[Dye]_{Total} \bullet \chi_{eq}(1 - e^{-kt})$ with an accompanying term *i.e.* $[Dye]_{Total} \bullet \chi_{NS}$, which accounts for the fraction of dye that is aggregated or non-specifically bound to the surface. In this case, the total dye loading was determined from the sum of the dye desorbed by the first desorption after 240 min in DMF/H_2O and the remaining dye desorbed in the TBAH/THF desorption (*c.f.* Section 2.4). The $[Dye]_{Total}$ determined experimentally was employed as a constant during the fitting process in order to determine the relative mole fraction of dye present at equilibrium in the solution (χ_{eq}) and the relative mole fraction of dye non-specifically bound to the surface (χ_{NS}).

$$[Dye]_{Total} = [Dye]_{Total}\,\chi_{eq}\left(1 - e^{-kt}\right) + [Dye]_{Total}\,\chi_{NS} \qquad (8)$$

In prior reports, the structure of the MK-2~TiO_2 interface was found to consist of a combination of strongly bound chemisorbed dye molecules forming a sub-monolayer with accompanying "non-specifically adsorbed" aggregate particles.[3, 13] The fraction of dye that is non-specifically adsorbed has been determined to be approximately 15 – 25%,[3] which is in excellent agreement with the results found herein (Table S1, χ_{NS}). The physisorbed dye is anticipated to rapidly dissolve into the solution upon immersion of the film into the water/DMF solution and can be considered as an offset to the overall desorption curve of the strongly bound dye layer. Therefore, it is also important to consider the percentage of the strongly bound dye that is desorbed in each experiment, since the strongly bound dye is expected to maintain the most efficient IET dynamics. Based on our experimentally determined kinetic parameters, the percent of the strongly bound dye desorbed in 0.1, 0.5 and 1.0 vol% of water in DMF is shown for the MK-2 and MK-2HA films in Table S1. Collectively, the results are consistent with the overall desorption results and suggest that the MK-2HA sensitized films are more stable to the presence of water. In addition, $[Dye]_{Total}$ and χ_{NS} are similar between the MK-2 (0.110 ± 0.003 μmol/cm^2 & 0.17 ± 0.02) and MK-2HA (0.082 ± 0.002 μmol/cm^2 & 0.21 ± 0.03) confirming that electrode preparation is reproducible.

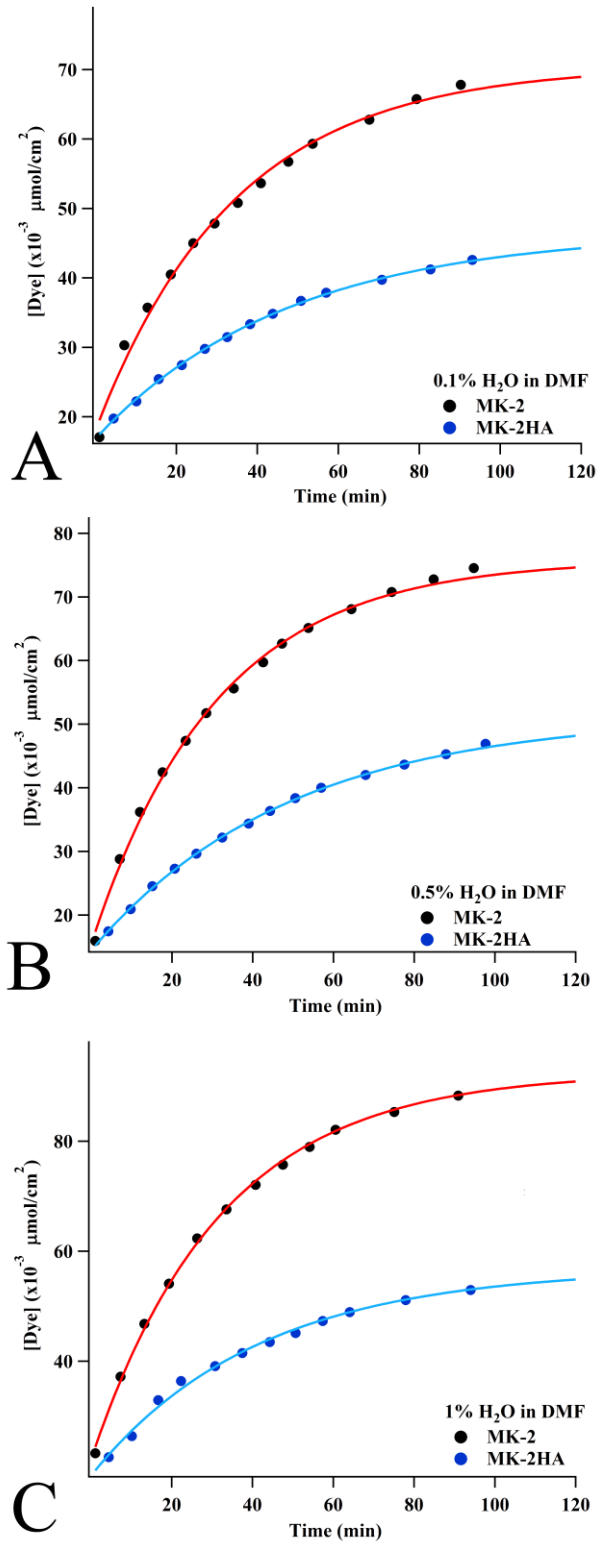

Figure S10. Desorption data with the associated fits to equation 6 overlaying the data in DMF with 0.1, 0.5 and 1% water (A – C), respectively.

Table S1.

Water Content (%)	Sensitizer	k (min^{-1})	χ_{eq}	χ_{NS}	Bound Dye Desorbed (%)
0.1 %	MK-2	0.029	0.49	0.17	59.0
	MK-2HA	0.021	0.372	0.210	47.1
0.5 %	MK-2	0.0323	0.556	0.142	64.8
	MK-2HA	0.0204	0.434	0.170	52.3
1.0 %	MK-2	0.0312	0.619	0.194	76.7
	MK-2HA	0.0243	0.47	0.240	61.8

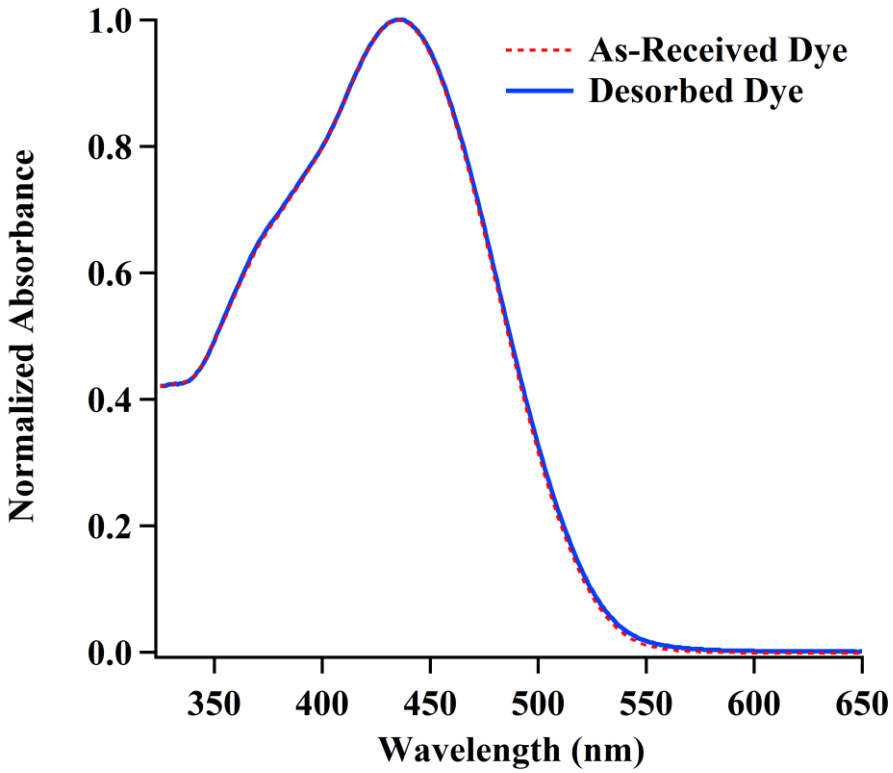

Figure S11. UV-visible spectra obtained from the solution obtained after desorbing a sensitized TiO_2 film in 1% water in DMF after a period of four hours, in comparison with a solution of the as-received commercial dye separately dissolved in 1% water in DMF.

7. Water Stability & Long-Term Durability of DSSC Devices as a Function of Hydroxamate and Carboxylate Anchoring Groups

Statistical Analysis of Long Term Stability Data: Each point in Figures 6 and 7 represents the mean obtained for measurements on three separate DSSC devices (that is, not merely multiple measurements on the same device). The associated standard deviations are shown in Figure S13 and S14. Our interest is in the overall trends in the photovoltaic parameters over the course of the 200 h test in order to compare the effect of increasing water content on solar cell performance when using different anchors. In some cases, a single data point deviates significantly from the overall trend, which could possibly be interpreted as either due to rapid changes in the actual solar cell parameters or due to random noise in the measurements.

We have employed a series of tests to determine if these point-to-point variations are statistically valid or are a result of inherent experimental noise. There are 24 data sets, each consisting of one photovoltaic parameter (efficiency, J_{sc}, FF, or V_{oc}), one percentage of water added (0%, 10%, 20%), one anchoring group (carboxylate or hydroxamate), and measurements taken after eight or nine different soaking durations.

Each data set was screened for potential outliers by determining if the mean value of a given point differed by more than one standard deviation from its adjacent points. Based on this screening, we employed the T-test to determine if the mean and standard deviation of an identified point indicated that it was drawn from a statistically different population from the rest of the points in the entire data set. Three points were identified in this manner: J_{sc} at 96 h for the anhydrous MK-2 cell, efficiency at 96 h for the anhydrous MK-2 cell, and the FF at 120 h for the 20% water MK-2 cell. The question then becomes whether or not the point in question truly is drawn from a statistically differing population.

To answer this, a Q-test was performed on all of the measurements in the data set containing the point in question (24 or 27 measurements depending on whether the length of the test was 168 or 192 hr) to determine if one of them is a statistical outlier. If so, that measurement was removed and the T-test described above was repeated on the point in question. In all cases, we find that removing a single individual outlier measurement results in a data set in which all points are drawn from a single population. Thus, we conclude that any large point-to-point variations in the plots shown in Figures 6, 7, S13, and S14 are due to random noise and not due to statistically meaningful differences.

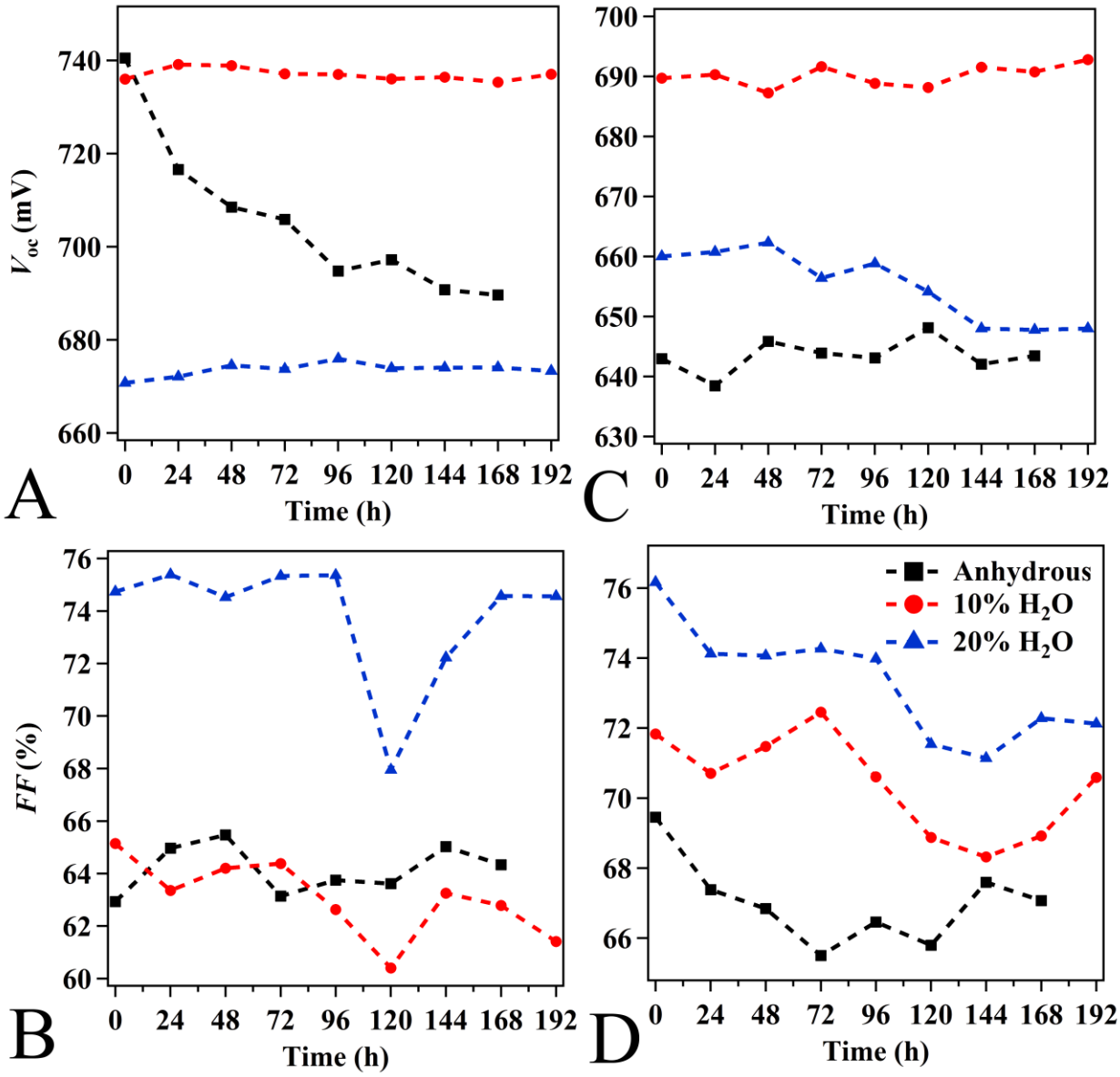

Figure S12. Time evolution of photovoltaic parameters including the V_{oc} (A & C) and *FF* (B & D) under one-sun simulated illumination for the MK-2 (A & B) and MK-2HA (C & D) devices containing specified amounts of water in electrolyte B.

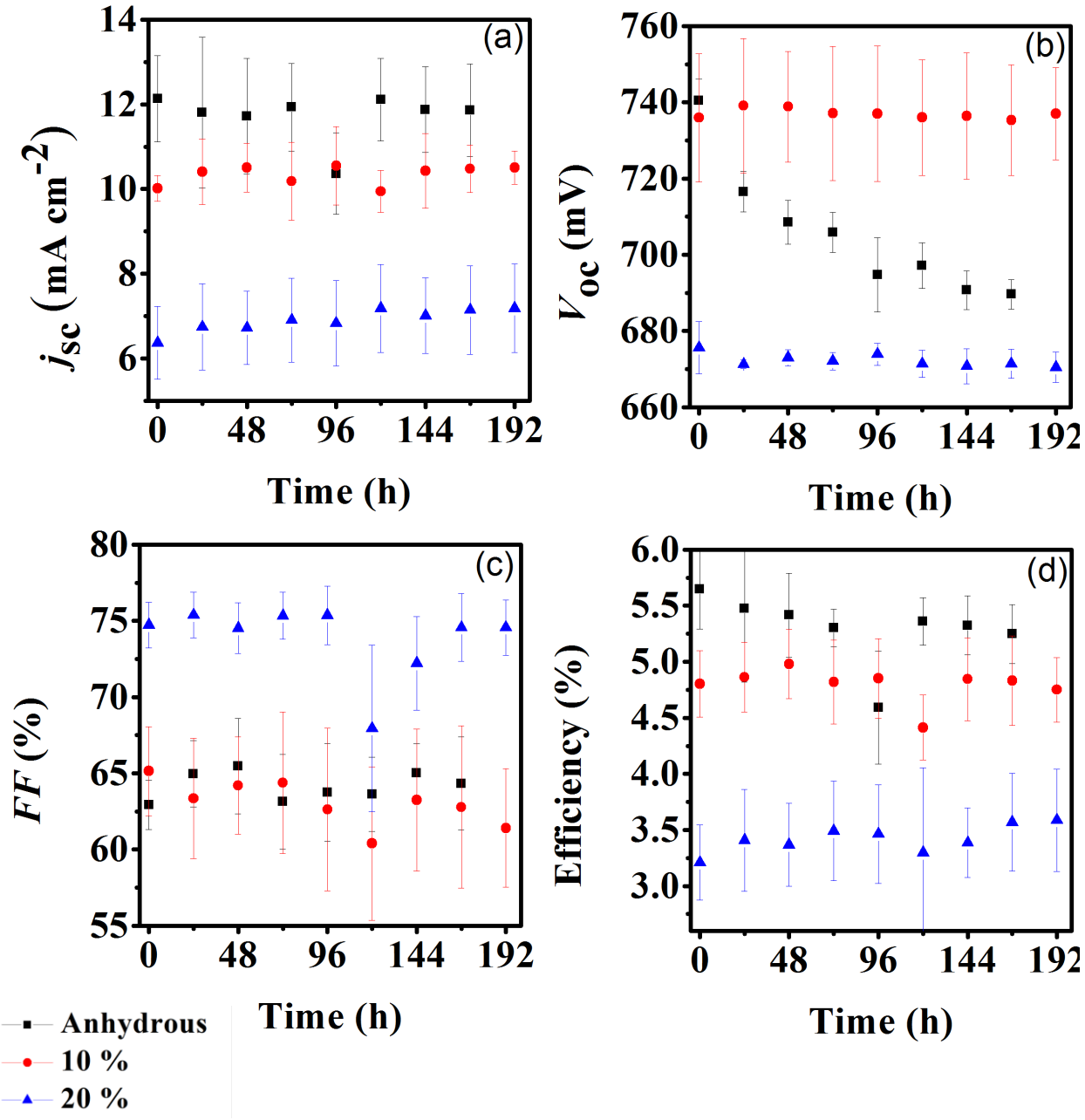

Figure S13. Time evolution of photovoltaic parameters under one-sun illumination for the MK-2 solar cells prepared with electrolyte B. After the *j-V* measurement, the devices were stored under dark conditions and at room temperature. Error bars are calculated from the standard deviation of the data collected from a minimum of four devices.

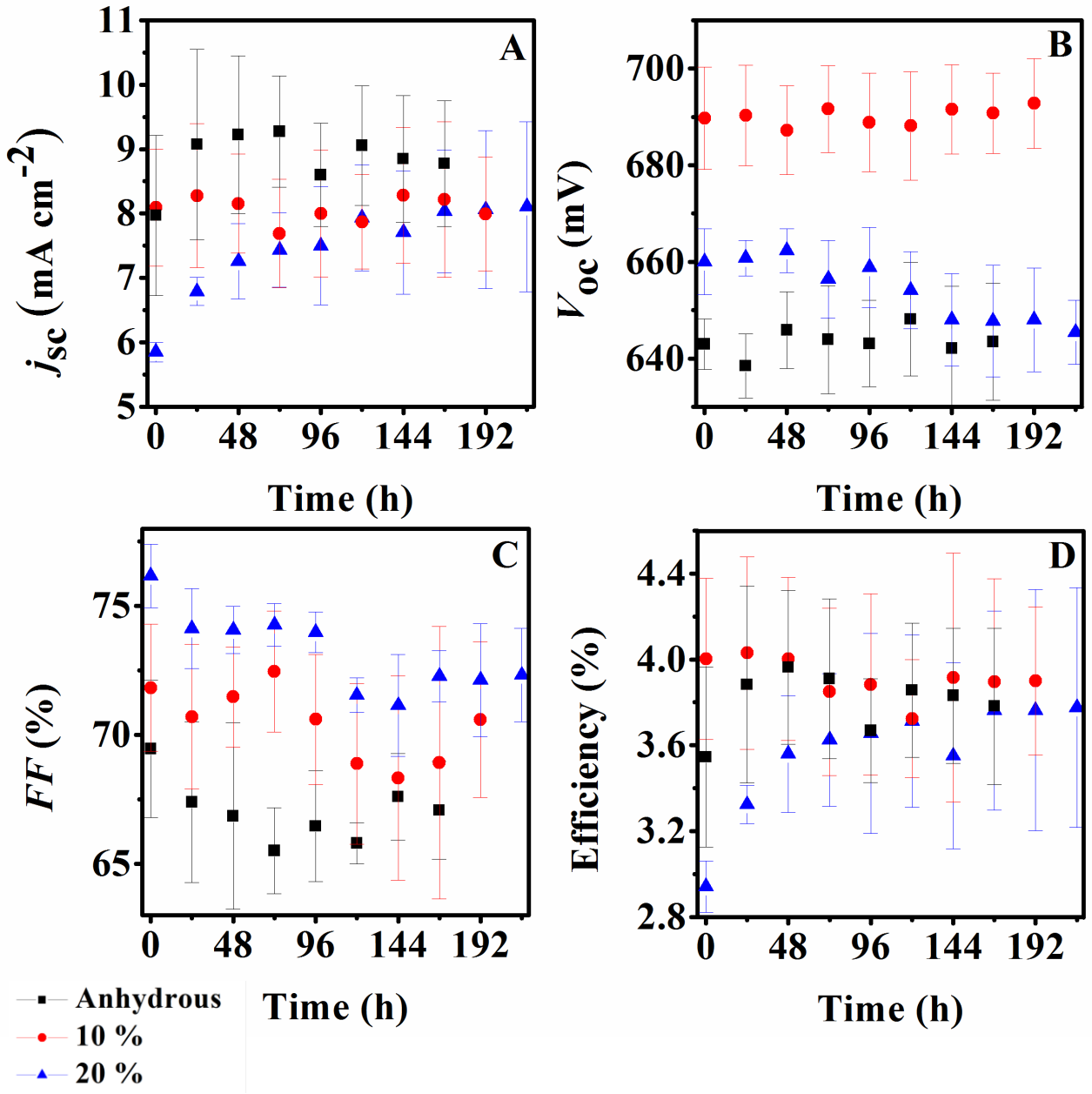

Figure S14. Time evolution of photovoltaic parameters under one-sun illumination for the MK-2HA solar cells prepared with electrolyte B. After the *j-V* measurement, the devices were stored under dark conditions and at room temperature. Error bars are calculated from the standard deviation of the data collected from a minimum of four devices.

8. References

1. K. Ngu and D. V. Patel, *J. Org. Chem.*, 1997, **62**, 7088-7089.
2. E. M. Barea, V. Gonzalez-Pedro, T. Ripolles-Sanchis, H. P. Wu, L. L. Li, C. Y. Yeh, E. W. G. Diau and J. Bisquert, *J. Phys. Chem. C*, 2011, **115**, 10898-10902.
3. Z.-S. Wang, N. Koumura, Y. Cui, M. Takahashi, H. Sekiguchi, A. Mori, T. Kubo, A. Furube and K. Hara, *Chem. Mater.*, 2008, **20**, 3993-4003.
4. M. Abrahamsson, P. G. Johansson, S. Ardo, A. Kopecky, E. Galoppini and G. J. Meyer, *J. Phys. Chem. Lett.*, 2010, **1**, 1725-1728.
5. W. R. McNamara, R. C. Snoeberger, G. Li, C. Richter, L. J. Allen, R. L. Milot, C. A. Schmuttenmaer, R. H. Crabtree, G. W. Brudvig and V. S. Batista, *Energy Environ. Sci.*, 2009, **2**, 1173-1175.
6. W. R. McNamara, R. L. Milot, H.-e. Song, R. C. Snoeberger Iii, V. S. Batista, C. A. Schmuttenmaer, G. W. Brudvig and R. H. Crabtree, *Energy Environ. Sci.*, 2010, **3**, 917-923.
7. C. J. Howard, T. M. Sabine and F. Dickson, *Acta Crystallographica Section B*, 1991, **47**, 462-468.
8. M. S. José, A. Emilio, D. G. Julian, G. Alberto, J. Javier, O. Pablo and S.-P. Daniel, *J. Phys.: Condens. Matter*, 2002, **14**, 2745.
9. J. P. Perdew, K. Burke and M. Ernzerhof, *Phys. Rev. Lett.*, 1996, **77**, 3865-3868.
10. M. J. Frisch, G. W. Trucks, H. B. Schlegel, G. E. Scuseria, M. A. Robb, J. R. Cheeseman, G. Scalmani, V. Barone, B. Mennucci, G. A. Petersson, H. Nakatsuji, M. Caricato, X. Li, H. P. Hratchian, A. F. Izmaylov, J. Bloino, G. Zheng, J. L. Sonnenberg, M. Hada, M. Ehara, K. Toyota, R. Fukuda, J. Hasegawa, M. Ishida, T. Nakajima, Y. Honda, O. Kitao, H. Nakai, T. Vreven, J. Montgomery, J. A., J. E. Peralta, F. Ogliaro, M. Bearpark, J. J. Heyd, E. Brothers, K. N. Kudin, V. N. Staroverov, R. Kobayashi, J. Normand, K. Raghavachari, A. Rendell, J. C. Burant, S. S. Iyengar, J. Tomasi, M. Cossi, N. Rega, J. M. Millam, M. Klene, J. E. Knox, J. B. Cross, V. Bakken, C. Adamo, J. Jaramillo, R. Gomperts, R. E. Stratmann, O. Yazyev, A. J. Austin, R. Cammi, C. Pomelli, J. W. Ochterski, R. L. Martin, K. Morokuma, V. G. Zakrzewski, G. A. Voth, P. Salvador, J. J. Dannenberg, S. Dapprich, A. D. Daniels, Ö. Farkas, J. B. Foresman, J. V. Ortiz, J. Cioslowski and D. J. Fox, Gaussian, Inc., Wallingford, CT, 2009, vol. Revision A.1.
11. L. G. C. Rego and V. S. Batista, *J. Am. Chem. Soc.*, 2003, **125**, 7989-7997.
12. A. Hagfeldt, G. Boschloo, L. Sun, L. Kloo and H. Pettersson, *Chem. Rev.*, 2010, **110**, 6595-6663.
13. A. B. Nepomnyashchii and B. A. Parkinson, *Langmuir*, 2013, **29**, 9362-9368.